Earth and Planetary Science Letters 381 (2013) 21–30

Contents lists available at ScienceDirect

Earth and Planetary Science Letters

www.elsevier.com/locate/epsl

The silicon isotopic composition of the Ganges and its tributaries

Guillaume Fontorbe [a], Christina L. De La Rocha [a], Hazel J. Chapman [b], Michael J. Bickle [b,*]

[a] UMR CNRS 6539, Institute Universitaire Européen de la Mer, Université de Bretagne Occidentale, Technôpole Brest-Iroise, Place Nicholas Copernic, 29280 Plouzané, France

[b] Department of Earth Sciences, University of Cambridge, Downing Street, Cambridge, CB2 3EQ, UK

ARTICLE INFO

Article history:
Received 15 September 2012
Received in revised form 26 July 2013
Accepted 13 August 2013
Available online 11 September 2013
Editor: G. Henderson

Keywords:
silicon isotopes
river chemistry
Ganges
Himalayas
chemical weathering

ABSTRACT

The silicon isotopic composition (δ^{30}Si) of the headwaters of the Ganges River, in the Himalaya, ranged from $+0.49 \pm 0.01$‰ to $+2.17 \pm 0.04$‰ at dissolved silicon (DSi) concentrations of 38 to 239 μM. Both the concentration and isotopic composition of DSi in the tributaries increased between the highest elevations to where the Ganges leaves the Himalayas at Rishikesh. The tributaries exhibit a linear correlation between δ^{30}Si and DSi that may represent mixing between a low DSi, low δ^{30}Si (e.g., 40 μM, +0.5‰) component potentially reflecting fractionation during adsorption of a small fraction of silicon onto iron oxides and a high DSi, high δ^{30}Si component (e.g., 240 μM, +1.7‰) produced during higher intensity weathering with a greater proportional sequestration of weathered silicon into secondary minerals or biogenic silica. On the Ganges alluvial plain, in the Ganges and the Yamuna, Gomati, and their tributaries, DSi ranged from 122 to 218 μM while δ^{30}Si ranged from $+1.03 \pm 0.03$‰ to $+2.46 \pm 0.06$‰. Highest values of δ^{30}Si occurred in the Gomati and its tributaries. In general, the lower DSi and higher δ^{30}Si of DSi in these rivers suggests control of both by removal of DSi by secondary mineral formation and/or biogenic silica production. A simple 1-dimensional model with flow through a porous medium is introduced and provides a useful framework for understanding these results.

1. Introduction

The two main inputs of dissolved silicon (DSi) to seawater are rivers (and groundwater) and deep sea hydrothermal vents (Tréguer et al., 1995; Slomp and Van Cappelen, 2004; Wheat and McManus, 2005; Laruelle et al., 2009; Dürr et al., 2011; Tréguer and De La Rocha, 2013) and the δ^{30}Si of seawater reflects the balance between the two (De La Rocha and Bickle, 2005). Currently, rivers and groundwater account for 70–85% of the DSi inputs (Tréguer et al., 1995; Tréguer and De La Rocha, 2013) and the average δ^{30}Si of seawater, in the neighborhood of +1‰ (De La Rocha et al., 2000; Wischmeyer et al., 2003; De La Rocha and Bickle, 2005), is closer to river values (0.0 to +3.4‰) (De La Rocha et al., 2000; Ding et al., 2004; Ziegler et al., 2005a, 2005b; Georg et al., 2006, 2007, 2009a; Cardinal et al., 2010) than hydrothermal ones (−0.3‰) (De La Rocha et al., 2000).

The elevated δ^{30}Si values of DSi in rivers compared to silicate rocks (generally between −0.3 and +0.2‰) (Douthitt, 1982; Ding et al., 1996; Ziegler et al., 2005a, 2005b; Georg et al., 2007; 2009b; Opfergelt et al., 2010, 2012; Savage et al., 2010, 2011; Pogge von Strandmann et al., 2012) reflect isotopic fractionation during addition and removal of DSi from soil, ground, and river waters during the dissolution of primary silicate minerals, the formation of secondary silicate minerals (clays), the adsorption of silicon onto iron oxide, the precipitation of siliceous cements (silcretes), and the formation and dissolution of biogenic silica (diatom frustules, sponge spicules, and phytoliths) in the terrestrial biogeosphere (Basile-Doelsch et al., 2005; Ziegler et al. 2005a, 2005b; Georg et al., 2006, 2007, 2009a, 2009b; Opfergelt et al., 2006, 2010; Ding et al., 2008; Delstanche et al., 2009; Pogge von Strandmann et al., 2012). Although these processes generally produce solid phases of low δ^{30}Si and therefore result in relatively high δ^{30}Si of DSi in rivers, the dissolution of clays of low δ^{30}Si can result in solutions of low δ^{30}Si (Ziegler et al., 2005a, 2005b; Georg et al., 2009a; 2009b; Cardinal et al., 2010). The same is true for the dissolution of phytoliths and other forms of biogenic silica (Opfergelt et al., 2006, 2010; Ding et al., 2008), a reservoir through which a significant portion of the reactive silicon in the terrestrial biogeosphere cycles (Conley, 2002; Laruelle et al., 2009). Further complicating the relationship between DSi and δ^{30}Si in rivers is that river waters are in transit, constantly mixing with waters of different origin and history, and composition, and subject to evaporation and rainfall.

It is equally important to quantify the various processes which control the δ^{30}Si of DSi in soil water, groundwater, and rivers and to study the cumulative effect of these processes in whole river

* Corresponding author. Tel.: +44 0 1223 333400; fax: +44 0 1223 333450.
E-mail address: mb72@esc.cam.ac.uk (M.J. Bickle).

0012-821X
http://dx.doi.org/10.1016/j.epsl.2013.08.026

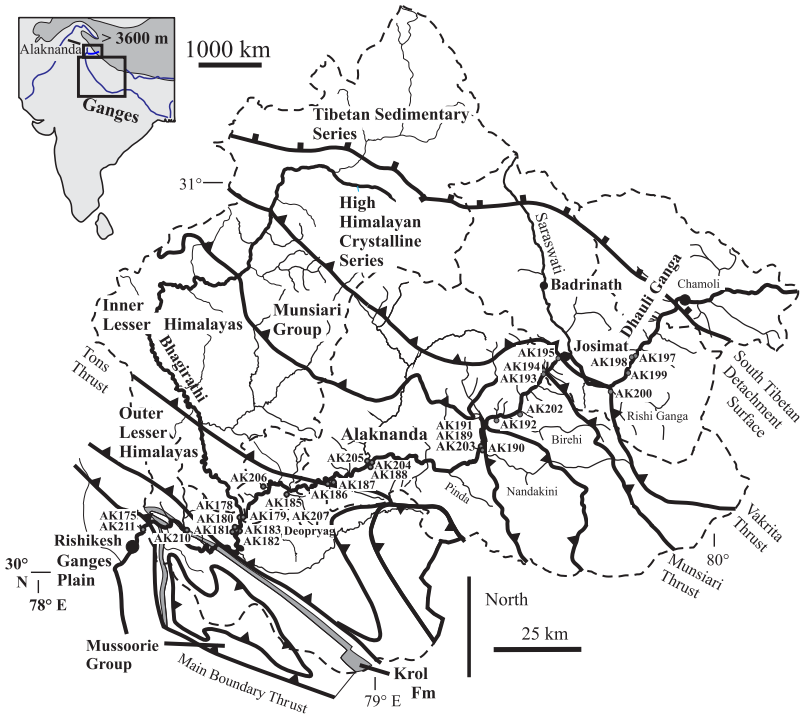

Fig. 1. Sampling locations in the headwaters of the Ganges, the more detailed map covering the area covered by the smaller box on the inset map of India. The larger box on the inset is detailed in Fig. 2. This geologic map is based on those presented by Bickle et al. (2001, 2003).

systems. We have studied the δ^{30}Si of DSi of the Ganges River and several important tributaries in India in the Himalaya and on the Ganges alluvial plain (Ganges floodplain). This river system is currently responsible for slightly less than 10% of the riverine silicon inputs to seawater (Dürr et al., 2011), a non-trivial portion of the silica budget for the global ocean.

2. Study area

We sampled the mainstem and numerous tributaries in the headwaters of the Ganges River in the Garhwal Himalaya and the Ganges and several of its main tributaries and numerous smaller tributaries on the Ganges alluvial plain (Figs. 1 and 2). The samples (see Supplementary Online Material for the list of samples by location) were collected in August 2003 at high flow in the middle of the monsoon.

2.1. The Himalaya

The main stream (called the Dhauli Ganga above Josimat, the Alakananda between Josimat and Deopryag, and the Ganga below Deopryag where it joins the Bhagirathi), drains three main geologic units (Fig. 1). It rises in the Tibetan Sedimentary Series of predominantly low metamorphic grade carbonate and siliciclastic rocks which are Palaeozoic and Mesozoic in age. The river then passes through the amphibolite facies of the High Himalayan Crystalline Series (schists, granitic gneisses, meta-quartzites, leucogranites and minor calc-silicates), followed by the lower grade Lesser Himalayan Series (schists, phyllites, quartzites, calc-silicates, dolomites, and limestones) before the main stream arrives onto the Ganges alluvial plain at Rishikesh. All three sections are important sources of solutes, each providing roughly 30% of, for example, dissolved strontium carried by the main streams (Bickle et al., 2003). Two large tributaries (the Mandakini and the Nandakini, draining mainly Lesser Himalayan Series and minor High Himalayan Crystalline Series) and numerous small tributaries were also sampled in the Himalaya.

The Tibetan Sedimentary Series on the Tibetan Plateau, with its high average elevation of 4900 m, has a cold, dry climate, sparse vegetation, and little direct anthropogenic interference. The High Himalayan Crystalline Series, a fifth of which is under permanent snow, ice, or glacier cover, has steep relief, with elevations ranging from 7800 m down to 1200 m. The much lower and less steep Lesser Himalayan Series (average elevation 2500 m) is covered with alpine, temperate, and subtropical vegetation. Erosion rates range from 0.8 ± 0.3 mm yr^{-1} in the Lesser Himalayan Series to 1.2 ± 0.1 mm yr^{-1} in the Tibetan Sedimentary Series and 2.7 ± 0.3 mm yr^{-1} in the High Himalayan Crystalline Series (Vance et al., 2003).

2.2. The Ganges alluvial plain

On the Ganges alluvial plain, the Ganges was sampled at Rishikesh, near Allahabad, and Varanasi, and, while the Yamuna itself was not sampled for isotopes, several of its larger tributaries were (Fig. 2). The chemistry of these major rivers reflects the inputs from the Himalayas and from additional weathering of Himalayan-derived sediment in the floodplain as well as lesser contribution from tributaries from the south which rise on the Deccan traps and flow across part of the Indian shield before entering the floodplain. The Yamuna River, the largest tributary of the Ganges, merges with the Ganges at Allahabad, contributing 60% to their combined flow.

Weathering processes in the floodplain were characterized by sampling the Gomati river and smaller tributaries which rise in the flood plain. The Gomati river drains an interfluve region between the Ganga and Ghaghara Rivers and lacks a direct Himalayan influence, although the complex irrigation network on the floodplain and a copious supply of water from the mountains makes it likely that all the rivers in the floodplain have some contribution from mountains. After originating in a swampy region near Puranpur, the Gomati flows ~900 km through alluvial plains consisting of fine sands and silty muds with discontinuous calcrete horizons (Singh, 1996). It drains an area of 30,437 km^2, a catchment with a

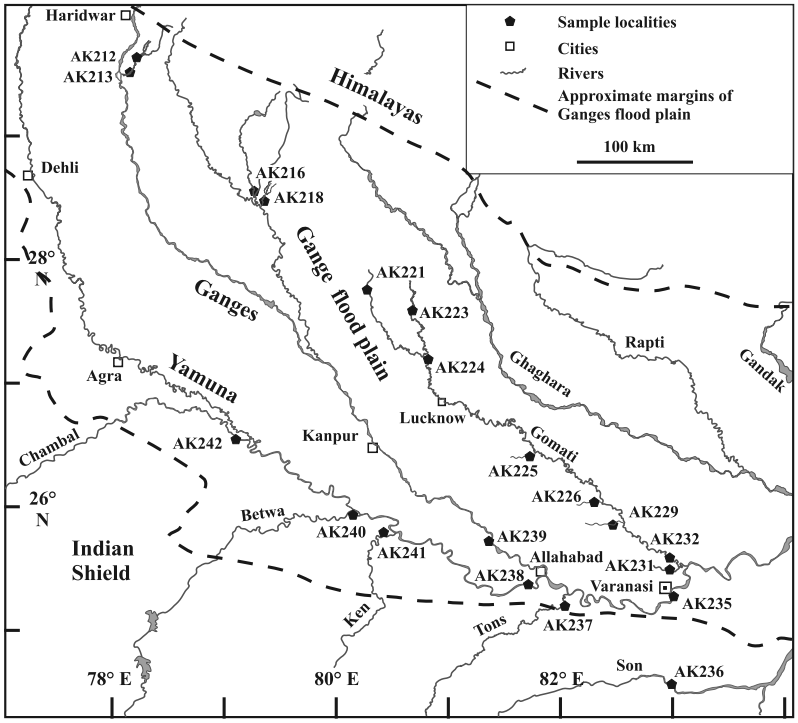

Fig. 2. Sampling locations on the Ganges alluvial plain. Location shown as the larger box on the inset on Fig. 1.

humid sub-tropical climate with hot summers, cooler winters, and heavy precipitation during the summer monsoon, before joining the Ganges near Saidpur (Singh et al., 2005) (Fig. 2). The Gomati is also polluted, receiving inputs from numerous cities and settlements, intensive agriculture, and distilleries and sugar factories.

3. Material and methods

Water samples were collected between the 12th and 28th of August, 2003. Samples for DSi concentrations and the δ^{30}Si of DSi (see Supplementary Online Materials for data tables) were immediately filtered through 0.6 µm polycarbonate filters (Poretics) and stored in the dark at ambient temperature in acid-cleaned LDPE bottles. Samples for anions and cations (see Supplementary Online Materials for data tables) were immediately filtered through 0.1 µm cellulose nitrate filters. One 30-mL fraction of the filtrate was acidified with quartz-distilled HCl to maintain a pH <2 prior to measurement of cations and one 20-mL fraction was stored unacidified for analysis of anions. Temperature and pH were measured at the time of collection.

Analyses of major and minor cations (Ca, Mg, Na, K, Al, Sr), S, and Si were made by AES and anions Cl, SO_4, and NO_3 by ion chromatography (methods in Supplementary material). DSi concentrations were measured on the samples collected for silicon isotopic analysis by molybdate blue spectrophotometry (Strickland and Parsons, 1972) and the mean difference between the AES and spectrophotometric analyses was $3.6 \pm 1.4\%$ (1σ).

Following prolonged storage in the dark to allow dissolved organic matter (DOM) to decay, silicon isotope samples were preconcentrated by adding 55 mM magnesium to each sample. Magnesium hydroxide, $Mg(OH)_2$, was precipitated by adding 2% by volume of 1 M NaOH to bring the pH above 10 (Karl and Tien, 1992). Silicon co-precipitates with the $Mg(OH)_2$, which was concentrated by centrifugation. Quantitative (100%) recovery of the DSi was obtained by a second round of precipitation. The collected precipitate was dissolved by using 1 M HCl to bring the pH below 2.

This concentrated Si was loaded onto ion exchange columns filled with AG1 X-8 resin (BioRad) following the protocol outlined in Engström et al. (2006) and utilized previously in the lab (De La Rocha et al., 2011), except that columns were preconditioned with 2 M HCl. Matrix elements were eluted with solutions of 95 mM HCl plus 23 mM HF. Purified Si was eluted with 5.6 mM HF in 0.14 M HNO_3. The acids used were all Suprapur (Merck) grade and were diluted with deionized distilled water (18.2 MΩ-cm).

The silicon isotopic composition of the samples was measured using a Neptune multi-collector inductively coupled plasma mass spectrometer (MC–ICPMS) (Thermo Scientific) at Ifremer (Brest), the Si solutions were diluted with 0.16 M nitric acid to 2.5 ppm Si to give a 10 V signal on mass 28 at medium resolution (see Table 3 in Supplementary Online Materials for additional information). The signal intensity of samples and standards (NBS28 and a laboratory working standard of 99.995% pure silica sand (Alfa Aesar)) was matched within 10% and all analyzed solutions contained the same amount of HF (~1 mM HF). Magnesium was added to the samples and the standards to give a concentration of 0.1 ppm. For each measurement, beam intensities at masses 25 and 26 (Mg), and 28, 29, and 30 (Si) in dynamic mode were monitored for 1 block of 30 cycles of 8 s integrations. Following each sample or standard was 5 min of rinse with 2% nitric acid.

Si isotope ratios ($^{30}Si/^{28}Si$ and $^{29}Si/^{28}Si$) were corrected for mass bias within the mass spectrometer by Mg-correction (Cardinal et al., 2003). The corrected ratio of ^{30}Si to ^{28}Si ($^{30}Si/^{28}Si)_{corr}$, is:

$$\left(\frac{^{30}Si}{^{28}Si}\right)_{corr} = \left(\frac{^{30}Si}{^{28}Si}\right)_{meas} \times \left(\frac{^{30}Si_{AM}}{^{28}Si_{AM}}\right)^{\varepsilon_{Mg}} \quad (1)$$

where $(^{30}Si/^{28}Si)_{meas}$ is the measured ratio of ^{30}Si to ^{28}Si and $^{28}Si_{AM}$ and $^{30}Si_{AM}$ are the atomic masses of ^{28}Si and ^{30}Si. The value of ε_{Mg} is calculated from the beam intensities on masses 25 and 26:

$$\varepsilon_{Mg} = \ln\left[\frac{\frac{^{25}Mg_A}{^{26}Mg_A}}{\left(\frac{^{25}Mg}{^{26}Mg}\right)_{meas}}\right] \div \ln\left[\frac{^{25}Mg_{AM}}{^{26}Mg_{AM}}\right] \quad (2)$$

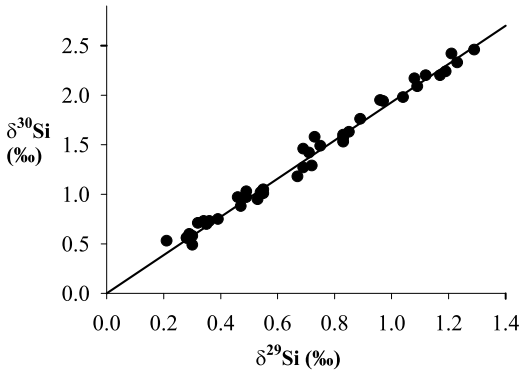

Fig. 3. Values of δ^{30}Si and δ^{29}Si of the samples fall along the expected mass-dependent fractional line of $\delta^{30}\text{Si} = 1.93(\delta^{29}\text{Si})$.

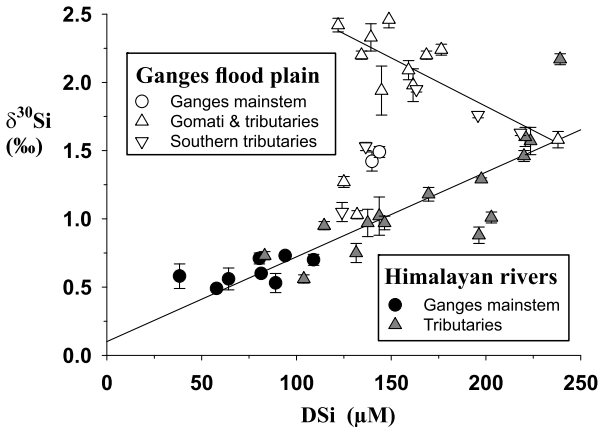

Fig. 4. δ^{30}Si plotted against concentrations of dissolved silicon (DSi) for all sites. When larger than the symbols, the $1-\sigma$ standard deviation of multiple analyses is shown. The trendline shown for the Himalayan rivers is $\delta^{30}\text{Si} = 0.006[\text{DSi}] + 0.10$ ($r^2 = 0.77$). The trendline for the upper set of floodplain rivers is $\delta^{30}\text{Si} = -0.007[\text{DSi}] + 3.25$ ($r^2 = 0.69$).

where $(^{25}\text{Mg}/^{26}\text{Mg})_{\text{meas}}$ is the measured ratio, $^{25}\text{Mg}_\text{A}/^{26}\text{Mg}_\text{A}$ is the ratio expected based on the natural abundances of the isotopes, and $^{25}\text{Mg}_\text{AM}$ and $^{26}\text{Mg}_\text{AM}$ are the atomic masses of ^{25}Mg and ^{26}Mg.

Corrected ratios were used to calculate the average δ^{30}Si and δ^{29}Si resulting from a series of bracketed standard-sample-standard measurements (generally comprising 2 blocks of the sample ratio and 3 of the standard ratio):

$$\delta^{x}\text{Si} = \frac{R_{\text{sam}} - R_{\text{std}}}{R_{\text{std}}} \times 10^3 \quad (3)$$

where δ^{x}Si is either δ^{29}Si or δ^{30}Si, and R_{sam} and R_{std} are either the ^{29}Si/^{28}Si of the sample and standard (for δ^{29}Si) or the ^{30}Si/^{28}Si of the sample and standard (for δ^{30}Si).

The precision for individual measurements was ±0.04‰ (1σ standard deviation) on δ^{30}Si. The long term precision (also 1σ SD) on the measurement of δ^{30}Si (including the column chemistry) was ±0.07‰, based on 22 standards measured between July 6, 2009 and September 1, 2010. Backgrounds and procedural blanks were generally less than 1% of the sample signal. Values fell along the expected mass dependent fractionation line $\delta^{30}\text{Si} = 1.93(\delta^{29}\text{Si})$ (Fig. 3).

4. Results

Weathering consists of two main processes with opposite effects, (1) the dissolution of Si (and other elements) from primary minerals to produce solutes, and (2) the removal of solutes to secondary phases such as clays. Weathering intensity refers to the degree of completeness to which an array of available primary minerals has been dissolved during weathering. Weathering rates refers to the rate of delivery (flux), e.g., of silicon out of rocks to solution per unit area and time.

4.1. The concentration and δ^{30}Si of dissolved silicon in the Himalayan rivers

In Himalayan mainstem (including the Ganges at Rishikesh) and smaller Himalayan tributaries, DSi concentrations ranged from 38 to 239 μM while the δ^{30}Si of DSi ranged from +0.49 ± 0.01‰ to +2.17 ± 0.04‰ (samples AK175 to AK211). On the Ganges alluvial plain (samples AK212 to AK242), DSi ranged from 122 to 218 μM and δ^{30}Si ranged from +1.03 ± 0.03‰ to +2.46 ± 0.06‰. The averages for the whole dataset are 134 ± 55 μM DSi and 1.3 ± 0.6‰ δ^{30}Si.

The Himalayan rivers show a positive correlation ($r^2 \sim 0.8$) between DSi concentration and δ^{30}Si (Fig. 4), suggesting that δ^{30}Si in the waters increases as dissolved Si concentrations increase as a result of progressive chemical weathering of silicate minerals. Alternatively, there could be systematic changes in the proportions of two components contributing to the tributary waters, one with low dissolved Si concentration and low δ^{30}Si and one with high dissolved Si and high δ^{30}Si (cf. Georg et al., 2006).

The small tributaries generally exhibit increasing DSi and δ^{30}Si with proximity to Rishikesh at the base of the Himalaya (Fig. 5). The 5 samples that do not fit this trend cluster near the village of Deopryag in the Outer Lesser Himalaya. One of these tributaries is not strictly small, but the Bhagirathi, which joins the Alaknanda mainstem at Deopryag roughly equal in terms of volume, distance traversed, and range of altitudes drained (Fig. 1). Without these samples, the relationship between distance towards Rishikesh and δ^{30}Si in small tributaries is strongly significant ($\delta^{30}\text{Si} = 0.006^*(\text{km}) + 2.45$; $r^2 = 0.78$; $n = 11$; $\alpha \leqslant 0.01$).

Unsurprisingly, DSi increases less steeply (and δ^{30}Si slightly) towards Rishikesh in the mainstem than in the tributary sample set (tributaries were generally each sampled at only one location which was close to their confluence with the mainstem). Tributaries drain smaller, more restricted catchments, with tributaries closer to Rishikesh draining warmer, lower elevation catchments (and thus representing the weathering processes in warmer, lower elevation catchments) than tributaries higher up in the Himalayas (i.e. further from Rishikesh on Fig. 5). The mainstem, in contrast, represents an averaging of all the inputs from above any particular sampling point. Bickle et al. (2003) estimated that the major water inputs to the Alaknanda in the monsoon were in the High Himalayas and the Lesser Himalayas above Deopryag. Given this, the change in Si and Si-isotopic composition downstream from the High Himalayas at 50 μM and 0.50‰, to 90 μM and ~0.56‰ at Deopryag and to ~100 μM and 0.75‰ at Rishikesh reflects the progressive inputs of higher DSi and δ^{30}Si silicon from the tributaries downstream. Variations such as the high δ^{30}Si of 0.71‰ at Rudrapryag probably reflect spatially localized storm inputs.

Annual average temperatures (represented by stream temperatures at the time of sampling in Figs. 5C and 6) also decrease with altitude in the Himalaya. This pattern is consistent with a relationship between Si concentration, δ^{30}Si and weathering intensity as conditions shift from sparsely-vegetated glacial to sub-tropical. No clear relationship is apparent between stream pH and DSi or δ^{30}Si.

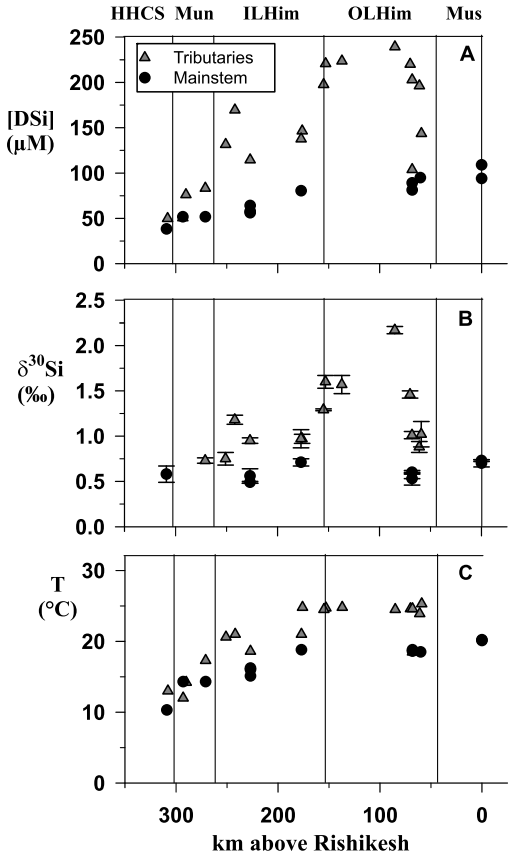

Fig. 5. The (A) concentrations of dissolved silicon (DSi), (B) δ^{30}Si of dissolved silicon, and (C) temperature in Himalayan tributaries and main streams versus distance from Rishikesh. Major tectonic units HHCS: High Himalayan Crystalline Series, Muns: Munsiari Group, ILHim: Inner Lesser Himalayan Series, OLHim: Outer Lesser Himalayan Series, Mus: Musoorie Group.

4.2. The concentration and δ^{30}Si of dissolved silicon in rivers of the Ganges alluvial plain

On the Ganges alluvial plain, DSi and δ^{30}Si exhibit no clear trend with distance from Rishikesh in either the mainstem or in the tributaries feeding into the Ganges (Fig. 7). Tributaries here have lower concentrations of DSi than the tributaries at lower elevations in the Himalayas. Overall, DSi in the alluvial plain tributaries gives the impression of a system where DSi concentrations are buffered to just below 150 µM, perhaps reflecting the removal of DSi by plants or secondary mineral formation. DSi in the Ganges mainstem, however, increase by approximately 40 µM between Rishikesh and the sites 700–900 km downstream northwest of Allahabad (AK239) and at Varanasi (AK235) (Fig. 7). The lack of mainstem samples over the 700 km interval mean that neither the manner of this increase (abrupt or gradual) nor its source (evaporative concentration, input from small, unsampled tributaries or groundwater, or input from weathering or dissolution of biogenic silica) can yet be identified.

The δ^{30}Si of different river systems on the Ganges alluvial plain are very similar. The δ^{30}Si of three small rivers within 250 km of Rishikesh (Fig. 7) falls between +1.0 and +1.6‰. Southern tributaries have slightly higher δ^{30}Si values, ranging from +1.0 to +2.0‰, averaging $+1.6 \pm 0.3$‰. The highest δ^{30}Si values of +1.9 and +2.5‰ (averaging $+2.2 \pm 0.2$‰) occur in the Gomati and its tributaries (Fig. 7).

DSi and δ^{30}Si in the Ganges mainstem increased between the beginning and end of the sampling path, with most of the increase in δ^{30}Si occurring on the Ganges alluvial plain. The mainstem evolved from low DSi (~50 µM) and δ^{30}Si (+0.6‰) high in the mountains, to intermediate DSi (~100 µM) but still low δ^{30}Si (+0.7‰) where the Ganga enters the alluvial plain at Rishikesh. The doubling of δ^{30}Si between Rishikesh and the further downstream sites (+1.5‰ near Allahabad and +1.4‰ at Varanasi) points to significant input of DSi with elevated δ^{30}Si from the alluvial plain and southern tributaries.

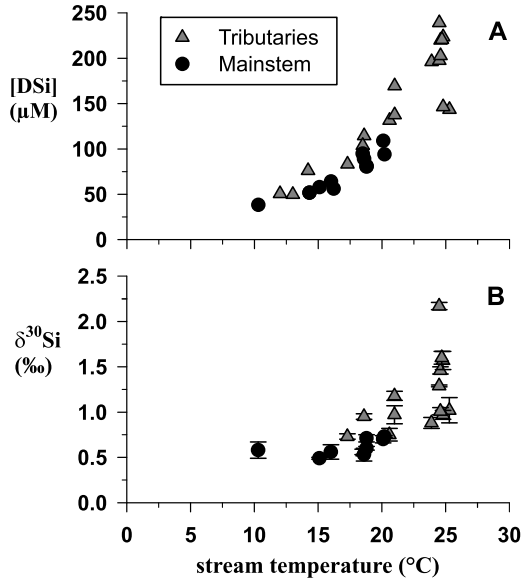

Fig. 6. (A) concentrations of dissolved silicon (DSi) and (B) the δ^{30}Si of dissolved silicon in smaller Himalayan tributaries and main streams versus stream temperature at the time of sample collection.

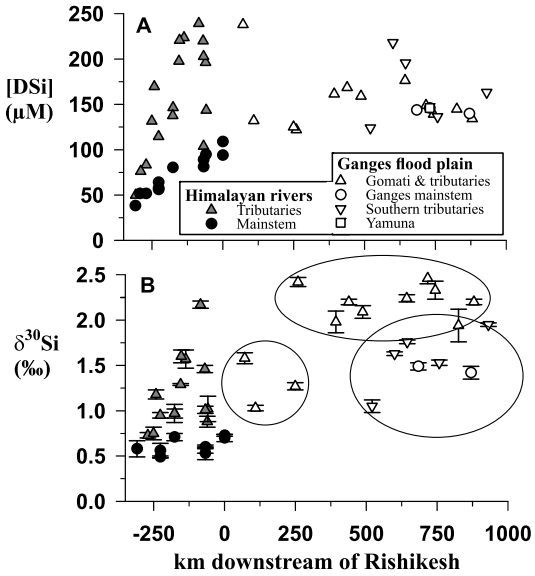

Fig. 7. (A) concentrations of dissolved silicon (DSi) and (B) δ^{30}Si of dissolved silicon for the entire sample set against distance from Rishikesh.

5. Discussion

5.1. The δ^{30}Si of dissolved silicon in the Ganges river system compared to other rivers

The average values of 134 ± 55 µM DSi and 1.3 ± 0.6‰ for δ^{30}Si for the Ganges river system are typical of rivers. The average DSi of world rivers is 160 µM (Dürr et al., 2011), with lower values found in cold, dry, high latitude regions and higher values

occurring in the hot, humid tropics. Values for the δ^{30}Si of DSi of +0.4 to +1.2‰ have been observed for temperate alpine rivers (De La Rocha et al., 2000; Georg et al., 2006), while values as high as +3.4‰ have been observed for the Yangtze, another temperate river (Ding et al., 2004). Lower values (e.g., around 0.0‰) have been reported in wetland rivers where considerable dissolution of clays occurs (Cardinal et al., 2010). Previously reported values from the Ganges river system include a sample of the mainstem Ganges, collected 130 km below Rishikesh at low flow, of +1.71‰ and a sample of the major Himalayan tributary, the Ghaghara river collected on the alluvial plain at Ayodhya, of +1.68‰ (Georg et al., 2009a). All these δ^{30}Si values are higher than those of primary silicate minerals (roughly −0.8‰ to +0.5‰; Douthitt, 1982; Ding et al., 1996; Savage et al., 2011), likely to be due to silicon isotope fractionation as weathered silicon is sequestered into clay minerals, biogenic silica, and other solid phases (De La Rocha et al., 2000; Ding et al., 2004, 2008; Ziegler et al., 2005a, 2005b; Georg et al., 2006, 2007, 2009a; 2009b; Opfergelt et al., 2006, 2010; Delstanche et al., 2009; Cardinal et al., 2010; Hughes et al., 2012; Pogge von Strandmann et al., 2012).

5.2. The relationships between the concentration and δ^{30}Si of dissolved silicon in the Ganges

In the samples from small Himalayan tributaries, δ^{30}Si increases with DSi and tributaries draining higher, cooler catchments have lower DSi and δ^{30}Si than those draining lower, warmer catchments. Fundamentally, at warmer temperatures and implied higher weathering intensities (i.e. a greater extent of dissolution of the suite of primary minerals available for weathering) solutions formed in weathering zones contain higher concentrations of solutes despite having lost a greater proportion of the weathered silicon to the formation of secondary minerals and/or biogenic silica. Previous observations of high δ^{30}Si corresponding to high solute concentrations during weathering (Pogge von Strandmann et al., 2012) directly support this idea. At cooler temperatures and lower weathering intensities, solutions have lower solute concentrations, including DSi, and less loss of silicon to secondary phases and thus lower δ^{30}Si. Depending upon location and catchment size, the tributaries reflect mixtures of solutions formed across a range of weathering intensities and little additional weathering occurs within them. The mainstem of the Ganges reflects a summation of the inputs of these various tributaries, meaning that multiple processes operating at different scales determine the DSi concentration and isotopic composition of the tributaries and mainstem of the Ganges. At its simplest, the composition of these streams reflects mixing of two basic end-member waters, one with high DSi and δ^{30}Si and the other with low DSi and δ^{30}Si, although it is more likely that there is a continuum of processes involved.

A similar positive, linear relationship between DSi and δ^{30}Si has been seen in other systems, for example in an alpine river, the Verzasca, although adjacent catchments behave differently. Georg et al. (2006) interpret the positive correlation to arise from mixing of the two end-members, with the high δ^{30}Si and high DSi end-member representing input at low flow, and the other, input at high flow. Similarly, a positive relationship between δ^{30}Si and DSi reported for tributaries of Lake Tanganyika, in Africa, has been interpreted to represent mixing between low δ^{30}Si, low DSi and high δ^{30}Si, high DSi endmembers (Alleman et al., 2005).

Stream chemistries in rapidly eroding sites in the Himalayas and Taiwan are best modeled by input from two or more components (Tipper et al., 2006; Calmels et al., 2011), further suggesting the correlation between δ^{30}Si and DSi in the Himalayan tributaries reflects a mixing of end-members. Mixing between an end-member of 240 µM DSi and +1.7‰ δ^{30}Si and one of 40 µM DSi and +0.5‰ δ^{30}Si would yield a linear relationship with slope

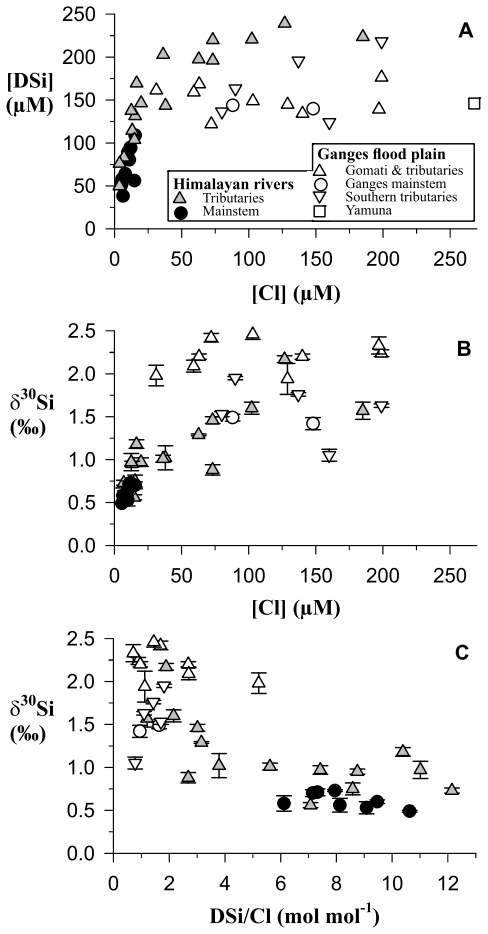

Fig. 8. (A) concentrations of dissolved silicon (DSi) plotted against chloride concentration, (B) the δ^{30}Si of dissolved silicon plotted against chloride concentration, and (C) the δ^{30}Si of dissolved silicon plotted against DSi/Cl for all samples.

0.006‰ µM^{-1}, the gradient observed in the Himalayan tributaries (Fig. 4). However, the Himalayan samples were collected over six days in August and DSi and δ^{30}Si may behave differently in different seasons or over longer periods.

Quantifying sequestration of silicon, weathered from primary silicates, into secondary phases like clays and biogenic silica would considerably advance our understanding of DSi and δ^{30}Si in the Himalayan rivers. Unfortunately, no known conservative tracer exists to correct DSi for dilution by rainfall or concentration via evaporation. Chloride, the most obvious candidate, is not added to Himalayan streams in a constant ratio with silicon due to inputs from the many hot springs (Bickle et al., 2003). This accumulating excess input of chloride is reflected in the curvature in the plot of DSi versus chloride (Fig. 8A). The general increase in δ^{30}Si with chloride (Fig. 8B) reflects the increase in δ^{30}Si with the input of solutes from weathering that is more strongly shown by δ^{30}Si versus DSi concentration (Fig. 4).

Concentrations of aluminum and Si/Al ratios have been proposed as tracers of secondary phase formation (Georg et al., 2006), but this will not work here. Firstly, the samples were not subject to ultra-filtration, potentially skewing the Al data due to its propensity to form colloids. Additionally, Al concentrations are strongly pH dependent and buffered by the precipitation of clays (which contain silicon) and by silicon-free phases such as gibbsite, $Al(OH)_3$. Lastly, the minimal solubility of Al means that dissolved Al concentrations poorly reflect the amount of Al dissolved during weathering reprecipitated as clay minerals and will be strongly dependent on the kinetics of these processes, although observations

of clay mineral saturation state suggest that natural waters are mostly saturated in the respective clay minerals (see Drever, 1997, Ch 12). It is unsurprising that in these samples, δ^{30}Si shows no variation over a broad range of Al concentrations above 1000 nM and, below 1000 nM Al, δ^{30}Si ranges broadly but with no systematic change in Al concentration (see Supplementary Online Materials for data).

5.3. Modeling of δ^{30}Si during fluid–rock reactions in weathering environments

Chemical weathering reactions take place as meteoric waters flow through soils, saprolites, and fractured bedrock. Inputs to tributaries and rivers consequently represent mixtures from a range of flow paths (cf. Calmels et al., 2011), with rocks also passing across the water flow paths, albeit more slowly, as the rocks are exhumed and progressively weathered. However, to illustrate the potential controls on the resulting isotopic composition of solutes like DSi, it is instructive to approximate weathering reactions by a simple 1-dimensional flow through a porous medium where the rates of fluid–mineral reactions are kinetically limited. Such modeling has successfully reproduced the sequence of mineral dissolution reactions and evolution of water chemistry in simple hydrological environments where water drains vertically through the weathered regolith nicely illustrated by the detailed studies on the soil chronosequences at Santa Cruz (White et al., 2008; Maher et al., 2009).

The evolution of Si concentrations and isotopic compositions are modeled along a 1-dimensional flow path, length z_1, in which water, with initial dissolved Si concentration C_0 and δ^{30}Si value $\delta_{\omega 0}$, is introduced at $z=0$ and minerals along the flow react at a constant rate to produce DSi at rate R_C (mol.m^{-3}.s^{-1}) of which $f.R_C$ is precipitated in secondary clay minerals, adsorbed onto iron oxides, or taken up by vegetation or siliceous microorganisms. This simple approximation, which ignores changes in reaction rate and reaction modes along the flow path or mixing of fluids from different flow paths, illustrates the fundamental controls on the evolution of silicon isotopic composition of the water that eventually ends up in streams.

The variation in DSi concentration C, with time t, and distance z, in a medium of porosity ϕ, in which fluid flows at velocity ω, is described by

$$\phi\frac{\partial C}{\partial t}=-\omega\phi\frac{\partial C}{\partial z}+(1-f)R_C \tag{4}$$

and the variation in δ^{30}Si in the water is given by

$$\phi\frac{\partial(C.\delta_w)}{\partial t}=\omega\phi\frac{\partial(C.\delta_\omega)}{\partial z}+R_C.\delta_r-f.R_C(\delta_\omega-\varepsilon) \tag{5}$$

where δ_r is the bulk δ^{30}Si of source minerals, δ_ω is the δ^{30}Si of the dissolved Si at distance z, ε is the bulk Si isotope fractionation (in ‰) between the DSi and that precipitated in secondary phases or biogenic silica. Isotopic compositions are treated as small numbers. For precipitation of multiple phases

$$\varepsilon=\sum\alpha_i.\varepsilon_i \tag{6}$$

where the sum is over i precipitating phases, each removing fraction α_i of the silicon precipitating with fractionation ε_i.

It is convenient to relate distance to the length of the flow path h, time to the transit time for water in the flow path and DSi concentration to the input concentration C_0, i.e.

$$\begin{aligned} z&=hz',\\ t&=\frac{h}{\omega}t',\\ C&=C_0C' \end{aligned} \tag{7}$$

which reduces Eq. (4) to

$$\frac{\partial C'}{\partial t'}=-\frac{\partial C'}{\partial z'}+N_D(1-f). \tag{8}$$

Eq. (8) is dependent on one dimensionless variable, a Damköhler-I number N_D (cf. Lassey and Blattner, 1988; Bickle, 1992; Maher, 2010) where

$$N_D=\frac{hR_C}{\omega\phi C_0}. \tag{9}$$

Eq. (5) reduces to

$$\frac{\partial(C'.\delta_w)}{\partial t'}=-\frac{\partial(C'.\delta_\omega)}{\partial z'}+N_D\big[\delta_r-f.(\delta_\omega+\varepsilon)\big]. \tag{10}$$

For flow through porous media where the proportion of reacting phases remains approximately constant and the porosities are relatively small, the time-dependent terms in Eqs. (4), (5), (8) and (9) are small compared to the advective and solid reaction-rate terms and may be ignored (the quasi-stationary state assumption; Lichtner, 1988). The trivial solution to Eq. (5) is then

$$C'=1+z'N_D(1-f) \tag{11}$$

and the solution to Eq. (10), given Eq. (11), is

$$\delta_\omega=(\delta_r-f\varepsilon)+\big(\delta_{\omega_0}-(\delta_r-f\varepsilon)\big).\big(1+z'N_D(1-f)\big)^{\left(\frac{1}{1-f}\right)} \tag{12}$$

where $\delta\omega_0$ is the initial isotopic composition of the fluid at $z'=0$.

Eq. (12) implies that waters evolve to a steady state Si-isotopic composition $(\delta_r-f\varepsilon)$ with a linear increase in DSi concentration with distance if $f<1$, that is if the fraction of silicon precipitated in secondary phases is less than that released by mineral dissolution. The monotonic increase in DSi concentrations will obviously be capped at higher DSi concentrations by an increase in the rate of silicon lost to secondary phases, i.e. f will tend to increase along flow paths. It should be noted that this model is not akin to the open system or continuous input zero-dimensional (box) model utilized frequently to describe the evolution of δ^{30}Si (or other isotopes) in the surface ocean (e.g., Barford et al., 1999; Varela et al., 2004; Cardinal et al., 2005; Georg et al., 2007; and many others) but only applicable to the non-steady state condition of ongoing net removal of the dissolved phase (Coffineau et al., 2013).

If secondary phases consume more Si than is released ($f>1$), the waters evolve towards $\delta_\omega=(\delta_r-f\varepsilon)$ at DSi = 0. For the special case that $R_C=0$, that is Si is removed from solution but no Si is supplied by dissolution the δ^{30}Si of the water can be described as classic Rayleigh distillation in a closed system (Hoefs, 2009)

$$\delta_\omega=\delta_{\omega_0}+\varepsilon\ln\big(1-N_Dz'\big). \tag{13}$$

The solutions (Eqs. (11) and (12)) imply that δ^{30}Si of DSi will evolve along convex paths against DSi concentration, the final isotopic composition dependent only on f, the fraction of dissolving Si reprecipitated, δ_r, the isotopic composition of the source minerals, and ε, the isotopic fractionation between silicon in solution and in precipitating phases (Fig. 9). The rate at which waters approach steady state isotopic compositions if $f<1$, or the limiting isotopic composition at DSi = 0 if $f>1$, depends on the Damköhler number, N_D. Since water Al concentrations are small, the 'f factors' are a function of the Si/Al ratios of the dissolving phases and the Si/Al ratios of the sum of the precipitating clay minerals and silcretes, Si adsorbed onto iron hydroxides and Si take up by vegetation. Table 1 lists f factors for the major silicate phases for precipitation of either kaolinite or a smectite with an estimate of the fraction of Si taken up by iron hydroxides for dissolution of iron-bearing minerals. For the latter, Table 1 adopts partition

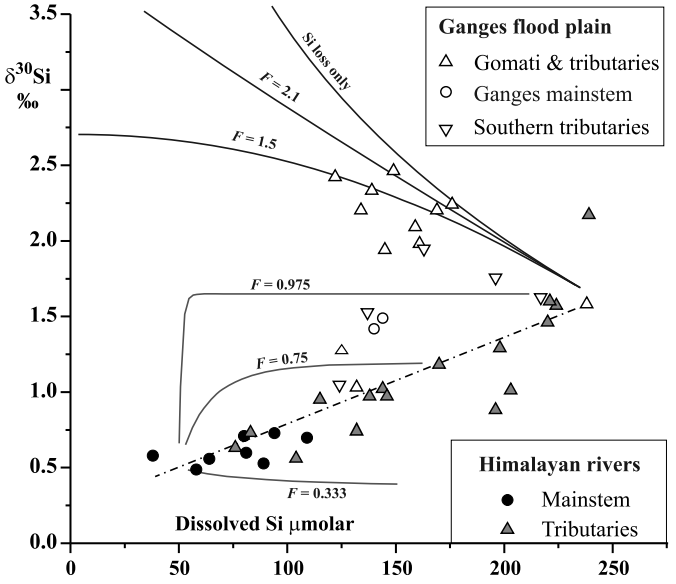

Fig. 9. Evolution of Si-isotope fractionations and Si concentrations calculated from one-dimensional flow modeling (Eqs. (11) and (12)) for a range of f values compared with analyses of Ganges river water samples. Solutions are shown for two starting compositions (1) fluid DSi = 50 µM and $\delta_{w0} = 0.5‰$ with $f < 1$ to simulate weathering in the Himalayas where weathering of higher Si/Al minerals to lower Si/Al clay minerals adds Si to waters and (2) fluid DSi = 230 µM and $\delta_{w0} = 1.4‰$ with $f > 1$ to simulate weathering in the Ganges alluvial plain where weathering reactions remove net Si from the waters. Note that in dissolved Si versus δ^{30}Si space the trajectories depend only on the f value but the distance the water compositions evolve along the trajectories is a function of the Damköhler number. It should be noted that f values probably also vary along flow paths, especially in higher Damköhler number settings where mineralogies and the weathering reactions evolve along the flow paths.

Table 1
f factors for different minerals.

f factors	Albite/K-spar	An33	Biotite	Muscovite	Chlorite
Kaolinite	0.33	0.50	0.59	0.85	1.11
Smectite	0.63	0.94	1.12	1.61	2.10
Fe-hydroxides			0.89		1.26

coefficients for silicon adsorption onto goethite and ferrihydrite fitted to the data of Delstanche et al. (2009) but these values must be considered uncertain as the surface area of the natural phases may differ from those synthesized in short term laboratory experiments.

The isotopic fractionations between waters and secondary phases are also uncertain. Delstanche et al. (2009) measured silicon isotopic fractionation (ε) of −1.04‰ for ferrihydrite and −1.56‰ for goethite. There are no satisfactory experimental data for equilibrium or kinetic controls on Si-isotopic fractionations associated with precipitation of clay minerals. Ziegler et al. (2005a) measured silicon isotope fractionation (ε) in the neighborhood of −2‰ for allophane (a precursor for kaolinite) in laboratory experiments, Georg et al. (2007) were able to model silicon fractionations during weathering of basalt to clay minerals on Iceland with $\varepsilon = -1.53‰$ and observations of isotopic fractionations in natural soils by Ziegler et al. (2005a, 2005b), Georg et al. (2006, 2009a, 2009b) and Opfergelt et al. (2010) are consistent with water – clay mineral silicon isotope fractionation in the range −1 to −3‰. Water-plant phytolith silicon isotope fractionations have been measured as −0.77‰ for bananas (Opfergelt et al., 2006) and water–marine diatom fractionation repeatedly at −1.1 to −1.5‰ (De La Rocha et al., 1997, 2011; Varela et al., 2004; Milligan et al., 2004; Cardinal et al., 2005; Reynolds et al., 2006; Fripiat et al., 2011).

5.4. Modeling of Si concentrations and isotopic compositions in the Gangetic rivers

Fig. 9 illustrates δ^{30}Si and DSi trends for weathering of silicate rock of $\delta^{30}Si = -0.3‰$ (best estimate for bulk Earth) with concurrent water-clay mineral isotopic fractionation of $\varepsilon = -2‰$ for a range of values of f, together with the data from the Himalayan and Ganges alluvial plain sampling locations. If the Himalayan crust had values slightly higher than this, reflecting the best estimates of crustal rocks (e.g. +0.1‰, Savage et al., 2010) the δ^{30}Si trends would just be displaced to higher values by the difference, that is +0.4‰. In reality, the sequence of weathering reactions will be more complex than the constant phase weathering illustrated in Fig. 9, but this exercise provides a framework to understand these more complex processes. Initial weathering reactions in the higher altitude catchments will involve very dilute solutions and rapid water transit times (low Damköhler number). At DSi concentrations below ∼50 µM, Al is deposited as $Al(OH)_3$ (gibbsite) (Drever, 1997, Fig. 10-6) and any silicon isotope fractionation is likely to reflect adsorption of silicon onto iron oxides. Above ∼50 µM DSi, kaolinite is the stable clay mineral and in the more rapidly eroding and cooler high-altitude catchments where plagioclase and biotite dissolution probably predominate, f and Damköhler numbers are probably both low, resulting in limited increases in both DSi and δ^{30}Si. At lower altitudes, in warmer and wetter catchments, weathering intensities increase (weathering intensity is the fraction of silicate minerals weathered) and there is proportionally more dissolution of the kinetically more sluggish minerals biotite, muscovite, and chlorite and K-feldspar than plagioclase. This will tend to increase the f factors, especially if the iron hydroxides produced by weathering of biotite and chlorite contribute to the removal of DSi. The progressive weathering at higher Damköhler numbers will produce more Si-rich waters and the higher f numbers, heavier δ^{30}Si compositions.

As is evident from Fig. 9, however, all this complexity might suggest that the Himalayan samples should display no simpler, linear trend between DSi concentrations and δ^{30}Si. The linear trend is likely to result from two component mixing (as proposed for an alpine river by Georg et al., 2006) between low Si, low δ^{30}Si and a higher Si, higher δ^{30}Si end-members where the proportion of the higher Si and δ^{30}Si end-member is higher in the more intensely weathered lower, warmer, and wetter catchments. The 1-D flow model presents an explanation for the generation of both the low DSi, low δ^{30}Si and the high dissolved silicon, high δ^{30}Si end-members.

The situation is different on the Ganges alluvial plain. Most of these rivers have DSi lower than the higher values observed in the Himalayan sample set (200 to 240 µM DSi). For these rivers, f factors exceed unity and further weathering precipitates more silicon than is released from primary minerals. This is the only mechanism which can drive the δ^{30}Si values up to between +1.9 and 2.5‰, well above the +1.7 to 2.1‰ limit that would be imposed by dissolution–precipitation of −0.3 to +0.1‰ silicate to clay minerals associated with an isotope fractionation (ε) of −2‰. Whether the lower DSi waters of the Ganges alluvial plain reflect removal of DSi by further weathering reactions (or production of biogenic silica) from higher DSi waters delivered from the mountains or more complete (intense) weathering of materials on the flood plain is unresolved, although changes in the elemental composition and hydration state of river sediments along the Ganges floodplain indicate that all of the above are occurring (Lupker et al., 2012). The increase in f above unity may reflect significant weathering of biotite, muscovite, and chlorite to smectite which has a significantly higher Si/Al ratio (1.8) than kaolinite (1.0), adsorption onto iron hydroxides, and/or uptake by vegetation and/or siliceous microorganisms. Smectite replaces kaolinite as the stable

clay mineral when waters reach about 900 µM DSi (Drever, 1997, Figs. 10-8, -9). This is much more concentrated than even the most enriched tributaries at high flow. However, Ganges alluvial plain groundwater samples reach this concentration, although they do not exhibit comparably high δ^{30}Si (Georg et al., 2009a, 2009b). As discussed above it, is probable that the trends of tributary samples on Fig. 9 reflect mixing of two or more water components with distinct compositions rather than the evolution of waters along an individual flow path. Georg et al. (2009a, 2009b) explain the low δ^{30}Si of the deeper groundwaters (0.04 and −0.2‰) as due to dissolution of secondary clay minerals or silcretes.

6. Conclusions

The evolution of DSi and δ^{30}Si of the set of tributaries in the Himalayan mountains and the Ganges flood plain exhibit consistent patterns, with DSi and δ^{30}Si increasing to a maximum of 250 µM and ∼1.5‰ in the lowest, warmest mountain tributaries but with DSi decreasing while δ^{30}Si continues to increase to roughly +2.2‰ in the flood plain. This is explained by weathering where an increasing fraction of Si is lost to secondary minerals or taken up by vegetation in the warmer catchments.

In general, weathering reactions and fluids will evolve along flow paths with dissolution of individual minerals taking place at different rates. The characteristics of such weathering profiles may be distinguished by their Damköhler numbers. In more mature and therefore higher Damköhler number profiles, a zone of completely reacted rock will develop near the start with primary minerals appearing at distances inversely proportional to their dissolution rates and fluids evolving so that they tend to equilibrium with the primary mineral assemblages in the more distal parts of the flow path. This is what is seen in the well studied chronosequences at Santa Cruz (e.g. White et al., 2008; Maher et al., 2009). Indeed Maher (2010) has argued that most chemical weathering takes place in flow paths with Damköhler numbers comparable to the Santa Cruz chronosequences, making the rates of such weathering reactions less sensitive to physical controls such as temperature. Prediction of the δ^{30}Si evolution along such a flow path is complex with initial fluids buffered by reactions with secondary minerals (which are of low δ^{30}Si) and by recycling by vegetation. Further into the profile, weathering of largely reacted (high weathering intensity) primary mineral assemblages might be expected to take place at relatively high f values followed by weathering of the more rapidly weathering plagioclase (lower f value) further into the profile, but with relatively evolved fluids. At greater distances, fluids will tend to chemical equilibrium with the primary mineral assemblages but it is doubtful that Si-isotopic exchange will take place in the absence of mineral reactions. This sort of weathering scenario would be expected to produce waters with roughly constant δ^{30}Si.

However the development of such 'complete' weathering profiles requires that the ratio of length of flow profile to water flux is high enough to maintain long fluid residence times and a high Damköhler number such as in the stable soil profiles developed in the Santa Cruz chronosequences. In high rainfall, high erosion rate environments, it is probable that fluid residence times are short and weathering takes place with low Damköhler numbers with low gradients in the modes of primary and secondary minerals with distance along the profiles. The modes of primary minerals would reduce with time at the expense of secondary minerals. In such a scenario δ^{30}Si isotopic compositions would be expected to evolve with time reflecting the changing 'f factors' of the assemblage (Fig. 9). The marked changes in δ^{30}Si across the Himalayan and Ganges alluvial flood plain samples would suggest that such a model is more appropriate for weathering in these environments where the variations reflect changes in the environmental parameters controlling weathering.

Acknowledgements

This research was funded was supported by grants from the Royal Society and the CNRS LEFE-CYBER program (to CDLR) and by NERC (Grant NE/B503741/1) (to MJB). We also thank Graham Howell (the Open University), Mervyn Greaves (University of Cambridge), and Emmanuel Ponzevera (Ifremer) for technical support and assistance.

Appendix A. Supplementary material

Supplementary material related to this article can be found online at http://dx.doi.org/10.1016/j.epsl.2013.08.026.

References

Alleman, L.Y., Cardinal, D., Cocquyt, C., Plisnier, P.-D., Descy, J.-P., Kimirei, I., Sinyinza, D., André, L., 2005. Silicon isotope fractionation in Lake Tanganyika and its main tributaries. J. Great Lakes Res. 31, 509–519.

Barford, C.C., Montoya, J.P., Altabet, M.A., Mitchell, R., 1999. Steady-state nitrogen isotope effects of N_2 and N_2O production in Paracoccus denitrificans. Appl. Environ. Microbiol. 65, 989–994.

Basile-Doelsch, I., Meunier, J.D., Parron, C., 2005. Another continental pool in the terrestrial silicon cycle. Nature 433, 399–402.

Bickle, M.J., 1992. Transport mechanisms by fluid-flow in metamorphic rocks: oxygen and strontium decoupling in the Trois Seigneurs massif – a consequence of kinetic dispersion?. Am. J. Sci. 292, 289–316.

Bickle, M.J., Harris, N.B.W., Bunbury, J., Chapman, H.J., Fairchild, I.J., Ahmad, T., 2001. Controls on the $^{87}Sr/^{86}Sr$ of carbonates in the Garwal Himalaya, headwaters of the Ganges. J. Geol. 109, 737–753.

Bickle, M.J., Bunbury, J., Chapman, H.J., Harris, N.B.W., Fairchild, I.J., Ahmad, T., 2003. Fluxes of Sr into the headwaters of the Ganges. Geochim. Cosmochim. Acta 67, 2567–2584.

Calmels, D., Galy, A., Hovius, N., Bickle, M., West, A.J., Chen, M.C., Chapman, H., 2011. Contribution of deep groundwater to the weathering budget in a rapidly eroding mountain belt, Taiwan. Earth Planet. Sci. Lett. 303, 48–58.

Cardinal, D., Alleman, L.Y., de Jong, J., Ziegler, K., André, L., 2003. Isotopic composition of silicon measured by multicollector plasma source mass spectrometry in dry plasma mode. J. Anal. At. Spectrom. 18, 213–218.

Cardinal, D., Alleman, L.Y., Dehairs, F., Savoye, N., Trull, T.W., André, L., 2005. Relevance of silicon isotopes to Si-nutrient utilization and Si-source assessment in Antarctic waters. Global Biogeochem. Cycles 19, GB2007, http://dx.doi.org/10.1029/2004GB002364.

Cardinal, D., Gaillardet, J., Hughes, H.J., Opfergelt, S., André, L., 2010. Contrasting silicon isotope signatures in rivers from the Congo Basin and the specific behaviour of organic-rich waters. Geophys. Res. Lett. 37, L12403, http://dx.doi.org/10.1029/2010GL043413.

Coffineau, N., De La Rocha, C.L., Pondaven, P., 2013. Exploring interacting influences on the silicon isotopic composition of the surface ocean: a case study from the Kerguelen Plateau. Biogeosci. Discuss. 10, 11405–11446.

Conley, D.J., 2002. Terrestrial ecosystems and the global biogeochemical silica cycle. Global Biogeochem. Cycles 16, 1121, http://dx.doi.org/10.1029/2002GB001894.

De La Rocha, C.L., Bickle, M.J., 2005. Sensitivity of silicon isotopes to whole-ocean changes in the silica cycle. Mar. Geol. 267, 267–282.

De La Rocha, C.L., Brzezinski, M.A., DeNiro, M.J., 1997. Fractionation of silicon isotopes by marine diatoms during biogenic silica formation. Geochim. Cosmochim. Acta 61, 5051–5056.

De La Rocha, C.L., Brzezinski, M.A., DeNiro, M.J., 2000. A first look at the distribution of the stable isotopes of silicon in natural waters. Geochim. Cosmochim. Acta 64, 2467–2477.

De La Rocha, C.L., Bescont, P., Croguennoc, A., Ponzevera, E., 2011. The silicon isotopic composition of surface waters of the Atlantic and Indian sectors of the Southern Ocean. Geochim. Cosmochim. Acta 75, 5283–5295.

Delstanche, S., Opfergelt, S., Cardinal, D., Elsass, F., André, L., Delvaux, B., 2009. Silicon isotopic fractionation during adsorption of aqueous monosilicic acid onto iron oxide. Geochim. Cosmochim. Acta 73, 923–934.

Ding, T., Jiang, S., Wan, D., Li, A., Li, J., Song, H., Liu, Z., Lao, X., 1996. Silicon Isotope Geochemistry. Geol. Publ. House, Beijing.

Ding, T., Wan, D., Wang, C., Zhang, F., 2004. Silicon isotope compositions of dissolved silicon and suspended matter in the Yangze River, China. Geochim. Cosmochim. Acta 68, 205–216.

Ding, T.P., Zhou, J.X., Wan, D.F., Chen, Z.Y., Wang, C.Y., Zhang, F., 2008. Silicon isotope fractionation in bamboo and its significance to the biogeochemical cycle of silicon. Geochim. Cosmochim. Acta 72, 1381–1395.

Douthitt, C.B., 1982. The geochemistry of the stable isotopes of silicon. Geochim. Cosmochim. Acta 46, 1449–1458.
Drever, J.I., 1997. The Geochemistry of Natural Waters, 3rd ed. Prentice Hall, Upper Saddle River.
Dürr, H.H., Meybeck, M., Hartmann, J., Laruelle, G.G., Roubeix, V., 2011. Global spatial distribution of natural riverine silica inputs to the coastal zone. Biogeosci. 8, 597–620.
Engström, E., Rodushkin, I., Baxter, D.C., Öhlander, B., 2006. Chromatographic purification for the determination of dissolved silicon isotopic compositions in natural waters by high resolution multicollector inductively coupled plasma mass spectrometry. Anal. Chem. 78, 250–257.
Fripiat, F., Cavagna, A.-J., Savoye, N., Dehairs, F., André, L., Cardinal, D., 2011. Isotopic constraints on the Si-biogeochemical cycle of the Antarctic Zone in the Kerguelen area (KEOPS). Mar. Chem. 123, 11–22.
Georg, R.B., Reynolds, B.C., Frank, M., Halliday, A.N., 2006. Mechanisms controlling the silicon isotopic composition of river waters. Earth Planet. Sci. Lett. 249, 290–306.
Georg, R.B., Reynolds, B.C., West, A.J., Burton, K.W., Halliday, A.N., 2007. Silicon isotope variations accompanying basalt weathering in Iceland. Earth Planet. Sci. Lett. 261, 476–490.
Georg, R.B., West, A.J., Basu, A.R., Halliday, A.N., 2009a. Silicon fluxes and isotope composition of direct groundwater discharge into the Bay of Bengal and the effect on the global ocean silicon isotope budget. Earth Planet. Sci. Lett. 283, 67–74.
Georg, R.B., Zhu, C., Reynolds, B.C., Halliday, A.N., 2009b. Stable silicon isotopes of groundwater, feldspars, and clay coatings in the Navajo Sandstone aquifer, Black Mesa, Arizona, USA. Geochim. Cosmochim. Acta 73, 2229–2241.
Hoefs, J., 2009. Stable Isotope Geochemistry, 6th ed. Springer. 300 pp.
Hughes, H.J., Bouillon, S., André, L., Cardinal, D., 2012. The effects of weathering variability and anthropogenic pressures upon silicon cycling in an intertropical watershed (Tana River, Kenya). Chem. Geol. 308–309, 18–25.
Karl, D.M., Tien, G., 1992. MAGIC – A sensitive and precise method for measuring dissolved phosphorus in aquatic environments. Limnol. Oceanogr. 37, 105–116.
Laruelle, G.G., et al., 2009. Anthropogenic perturbations of the silicon cycle at the global scale: Key role of the land-ocean transition. Global Biogeochem. Cycles 23, GB4031, http://dx.doi.org/10.1029/2008GB003267.
Lassey, K.R., Blattner, P., 1988. Kinetically controlled oxygen isotope exchange between fluid and rock in one-dimensional advective flow. Geochim. Cosmochim. Acta 52, 2169–2175.
Lichtner, P.C., 1988. The quasi-stationary state approximation to coupled mass transport and fluid rock interaction in a porous medium. Geochim. Cosmochim. Acta 52, 143–165.
Lupker, M., France-Lanord, C., Galy, V., Lavé, J., Gaillardet, J., Gajurel, A.P., Guilmette, C., Rahman, M., Singh, S.K., Sinha, R., 2012. Predominant floodplain over mountain weathering of Himalayan sediments (Ganga basin). Geochim. Cosmochim. Acta 84, 410–432.
Maher, K., 2010. The dependence of chemical weathering rates on fluid residence time. Earth Planet. Sci. Lett. 294, 101–110.
Maher, K., Steefel, C.I., White, A.F., Stonestrom, D.A., 2009. The role of reaction affinity and secondary minerals in regulating chemical weathering rates at the Santa Cruz Soil Chronosequence, California. Geochim. Cosmochim. Acta 73, 2804–2831.
Milligan, A.J., Varela, D.E., Brzezinski, M.A., Morel, F.M.M., 2004. Dynamics of silicon metabolism and silicon isotopic discrimination in a marine diatom as a function of pCO_2. Limnol. Oceanogr. 49, 322–329.
Opfergelt, S., Cardinal, D., Henriet, C., Draye, X., André, L., Delvaux, B., 2006. Silicon isotopic fractionation by banana (Musa spp.) grown in a continuous nutrient flow device. Plant Soil 285, 333–345.
Opfergelt, S., Cardinal, D., André, L., Delvigne, C., Bremond, L., Delvaux, B., 2010. Variations of δ^{30}Si and Ge/Si with weathering and biogenic input in tropical basaltic ash soils under monoculture. Geochim. Cosmochim. Acta 74, 225–240.
Opfergelt, S., Georg, R.B., Delvaux, B., Cabidoche, Y.-M., Burton, K.W., Halliday, A.N., 2012. Silicon isotopes and the tracing of desilication in volcanic soil weathering sequences, Guadeloupe. Chem. Geol. 326–327, 113–122.
Pogge von Strandmann, P.A.E., Opfergelt, S., Lai, Y.-J., Sigfússon, B., Gislason, S.R., Burton, K.W., 2012. Lithium, magnesium and silicon isotope behaviour accompanying weathering in a basaltic soil and pore water profile in Iceland. Earth Planet. Sci. Lett. 339–340, 11–23.
Reynolds, B.C., Frank, M., Halliday, A.N., 2006. Silicon isotope fractionation during nutrient utilization in the North Pacific. Earth Planet. Sci. Lett. 244, 431–443.
Savage, P.S., Georg, R.B., Armytage, R.M.G., Williams, H.M., Halliday, A.N., 2010. Silicon isotope homogeneity in the mantle. Earth Planet. Sci. Lett. 295, 139–146.
Savage, P.S., Georg, R.B., Williams, H.M., Burton, K.W., Halliday, A.N., 2011. Silicon isotope fractionation during magmatic differentiation. Geochim. Cosmochim. Acta 75, 6124–6139.
Singh, I.B., 1996. Geological evolution of Ganga Plain – an overview. J. Palaeont. Soc. India 41, 99–137.
Singh, M., Sharma, M., Tobschall, H.J., 2005. Weathering of the Ganga alluvial plain, northern India: implications from fluvial geochemistry of the Gomati River. Appl. Geochem. 20, 1–21.
Slomp, C.P., Van Cappelen, P., 2004. Nutrient inputs to the coastal ocean through submarine groundwater discharge: controls and potential impact. J. Hydrol. 295, 64–86.
Strickland, J.D.H., Parsons, T.R., 1972. A Practical Handbook of Seawater Analysis. Fish Res. Board, Canada.
Tipper, E.T., Bickle, M.J., Galy, A., West, A.J., Pomiès, C., Chapman, H.J., 2006. The short term climatic sensitivity of carbonate and silicate weathering fluxes: Insight from seasonal variations in river chemistry. Geochim. Cosmochim. Acta 70, 2737–2754.
Tréguer, P., Nelson, D.M., Van Bennekom, A.J., DeMaster, D.J., Leynaert, A., Quéguiner , B., 1995. The silica balance in the world ocean: A reestimat. Science 268, 375–379.
Tréguer, P.J., De La Rocha, C.L., 2013. The world ocean silica cycle. Annu. Rev. Mar. Sci. 5, 477–501.
Vance, D., Bickle, M.J., Ivy-Ochs, S., Kubik, P.W., 2003. Erosion and exhumation in the Himalaya from cosmogenic isotope inventories of river sediments. Earth Planet. Sci. Lett. 206, 273–288.
Varela, D.E., Pride, C.J., Brzezinski, M.J., 2004. Biological fractionation of silicon isotopes in Southern Ocean surface waters. Global Biogeochem. Cycles 18, GB1047, http://dx.doi.org/10.1029/2003GB002140.
Wheat, C.G., McManus, J., 2005. The potential role of ridge-flank hydrothermal systems on oceanic germanium and silicon balances. Geochim. Cosmochim. Acta 69, 2021–2029.
White, A.F., Schulz, M.S., Vivit, D.V., Blum, A.E., Stonestrom, D.A., Anderson, S.P., 2008. Chemical weathering of a marine terrace chronosequence, Santa Cruz, California I: Interpreting rates and controls based on soil concentration–depth profiles. Geochim. Cosmochim. Acta 72, 36–68.
Wischmeyer, A.G., De La Rocha, C.L., Maier-Reimer, E., Wolf-Gladrow, D.A., 2003. Control mechanisms for the oceanic distribution of silicon isotopes. Global Biogeochem. Cycles 17, 1083, http://dx.doi.org/10.1029/2002GB002022.
Ziegler, K., Chadwick, O.A., White, A.F., Brzezinski, M.A., 2005a. δ^{30}Si systematics in a granitic saprolite, Puerto Rico. Geology 33, 817–820.
Ziegler, K., Chadwick, O.A., Brzezinski, M.A., Kelly, E.F., 2005b. Natural variations of δ^{30}Si ratios during progressive basalt weathering, Hawaiian Islands. Geochim. Cosmochim. Acta 69, 4597–4610.